Selective Diagnosis of Diabetes Using Pt-Functionalized WO3 Hemitube Networks As a Sensing Layer of Acetone in Exhaled Breath

ARTICLE *in* ANALYTICAL CHEMISTRY · DECEMBER 2012

Impact Factor: 5.64 · DOI: 10.1021/ac303148a · Source: PubMed

7 AUTHORS, INCLUDING:

Ingun Lee
Korea Advanced Institute of Science and Tech…
3 PUBLICATIONS **108** CITATIONS

SEE PROFILE

Won-Hee Ryu
Yale University
42 PUBLICATIONS **500** CITATIONS

SEE PROFILE

analytical chemistry

Article

pubs.acs.org/ac

Selective Diagnosis of Diabetes Using Pt-Functionalized WO_3 Hemitube Networks As a Sensing Layer of Acetone in Exhaled Breath

Seon-Jin Choi, Inkun Lee, Bong-Hoon Jang, Doo-Young Youn, Won-Hee Ryu, Chong Ook Park, and Il-Doo Kim*

Department of Materials Science and Engineering, Korea Advanced Institute of Science and Technology (KAIST), Daejeon 305-701, Republic of Korea

Supporting Information

ABSTRACT: Thin-walled WO_3 hemitubes and catalytic Pt-functionalized WO_3 hemitubes were synthesized via a polymeric fiber-templating route and used as exhaled breath sensing layers for potential diagnosis of halitosis and diabetes through the detection of H_2S and CH_3COCH_3, respectively. Pt-functionalized WO_3 hemitubes with wall thickness of 60 nm exhibited superior acetone sensitivity (R_{air}/R_{gas} = 4.11 at 2 ppm) with negligible H_2S response, and pristine WO_3 hemitubes showed a 4.90-fold sensitivity toward H_2S with minimal acetone-sensing characteristics. The detection limit (R_{air}/R_{gas}) of the fabricated sensors with Pt-functionalized WO_3 hemitubes was 1.31 for acetone of 120 ppb, and pristine WO_3 hemitubes showed a gas response of 1.23 at 120 ppb of H_2S. Long-term stability tests revealed that the remarkable selectivity has been maintained after aging for 7 months in air. The superior cross-sensitivity and response to H_2S and acetone gas offer a potential platform for application in diabetes and halitosis diagnosis.

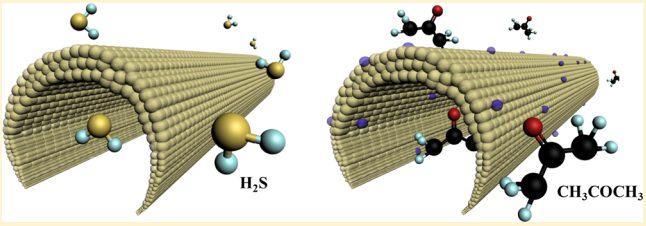

There are hundreds of species of volatile organic compounds (VOCs) in human breath; these compounds are exhaled from the blood through breath in the lungs.[1,2] The exact evaluation of the concentration of these VOC gases offers useful information that can be used to identify biomarkers for analyzing the human body condition. Disease diagnosis using exhaled breath has attracted much attention because of its key advantages in terms of noninvasive and real-time diagnosis. So far, gas chromatography/mass spectrometry (GC/MS)[1−3] and the optical spectroscopy method[4] have been widely used for breath analysis for potential detection of lung cancer,[1] diabetes,[5] heart disease,[6] malnutrition,[7] kidney disorders,[8] and asthma.[9] However, these techniques are limited for applications in portable sensing devices owing to the bulky equipment size and complexity in measurement.

To achieve accurate disease diagnosis using exhaled breath sensors, the minimum detection limit should be in the range of ppb (parts per billion) level, particularly in highly humid atmospheres. In addition, selective detection should be guaranteed to confirm exact recognition of a specific disease. For example, in the case of diabetes diagnosis, we should measure an acetone concentration of 300−900 ppb in exhaled breath because the acetone concentration increases from 300 to 900 ppb for healthy humans to 1800 ppb for diabetes patients.[10]

Chemiresistive type sensors using various semiconducting metal oxides, such as WO_3,[11] MoO_3,[12] SnO_2,[13,14] and NiO,[15] have been considered for use as exhaled breath sensors due to their superior reaction with VOCs, easy fabrication processes and possibility of miniaturization for integration in portable devices.[12,16] Thus far, several promising research efforts have been conducted for fabrication of highly sensitive exhaled breath sensors; in particular, by combining noble catalysts and unique metal oxide nanostructures that possess a high surface area and high porosity. These devices include Pd−TiO_2 nanofibers,[17] Pt− and IrO_2−WO_3 nanofibers,[18] Au−TiO_2 nanotubes,[19] and PdO−SnO_2 nanofibers.[20] However, accurate cross-sensitivity toward exhaled breath containing several gases such as acetone, H_2S, toluene, etc., is still a major challenge.

In this work, we fabricated thin-walled WO_3 hemitubes with different top wall thicknesses (121 and 58.6 nm) by utilizing electrospun nanofibers as a sacrificial template and performing subsequent RF-sputtering coating of WO_3 films on the polymeric fibers, followed by high temperature calcination (Figure S1 in the Supporting Information). Thin-walled WO_3 hemitubes (Scheme 1a) exhibited a superior gas response toward H_2S in 85% relative humidity, demonstrating potential feasibility for halitosis diagnosis. In contrast, catalytic Pt-functionalized WO_3 hemitubes showed remarkably enhanced acetone sensitivity while showing negligible H_2S sensing characteristics (Scheme 1b). We investigate the role of catalysts anchored to WO_3 hemitubes in selective detection of acetone and H_2S as biomarkers for diagnosis of diabetes and halitosis, respectively.

Figure 1 shows the schematic illustrations of pristine WO_3 hemitubes and Pt-functionalized WO_3 hemitubes. To synthe-

Received: October 29, 2012
Accepted: December 20, 2012
Published: December 20, 2012

   dx.doi.org/10.1021/ac303148a | *Anal. Chem.* 2013, 85, 1792−1796

Scheme 1. Schematic Illustrations of (a) Polycrystalline WO_3 Hemitube Optimized for H_2S Detection and (b) Pt-Functionalized WO_3 Hemitube for Selective Acetone Detection

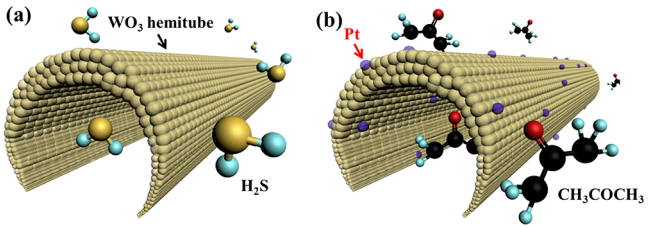

size a WO_3 hemitube structure, electrospun PVP (polyvinylpyrollidone)/PMMA (polymethylmethacrylate) composite nanofibers (Figure S2a in the Supporting Information) were coated by RF-sputtered WO_3 thin films (Figure S2b in the Supporting Information). Figure 1a shows a cross-sectional SEM image of 52.5 nm thick WO_3 (shell) films coated on a PVP/PMMA (core) nanofiber. An asymmetric tube structure was achieved after heat treatment at 500 °C as a result of the removal of the sacrificial templates and predominant deposition on the top surface of the electrospun fibers[21] (Figure 1b and c). Figure 1b shows that WO_3 hemitubes had a top wall thickness of 121 nm and a side wall thickness of 73 nm.

A shorter sputtering time induces a thinner wall thickness (top wall thickness, 58.6 nm; side wall thickness, 32.2 nm). To investigate the morphology and structure of the WO_3 hemitube in greater detail, transmission electron microscopy (TEM) analysis was performed (Figure 1e and f). Figure 1e shows a magnified image of a single WO_3 hemitube (Figure S3a in the Supporting Information). Figure 1d and e clearly verify the hemitubular nature of the thin-walled WO_3 films.

Selected area electron diffraction pattern analysis revealed that the WO_3 hemitube had characteristic peaks of (200) and (020) planes (Figure 1f), which correspond to interplanar distances of 3.67 Å and 3.75 Å, respectively, maintaining an angle of 90°. To improve the exhaled breath sensing characteristics, nanoscale Pt catalysts were functionalized on the inner and outer surfaces of the WO_3 hemitubes. We synthesized a colloidal Pt solution via a polyol process[22] and decorated Pt nanoparticles on the predrop-coated WO_3 hemitube networks. As indicated by the green arrow, both the inside and outside of the WO_3 hemitubes were functionalized by Pt catalysts (Figure 1g). High-resolution TEM analysis demonstrated that Pt catalysts with a size distribution of 3−7 nm were mostly attached to WO_3 hemitubes

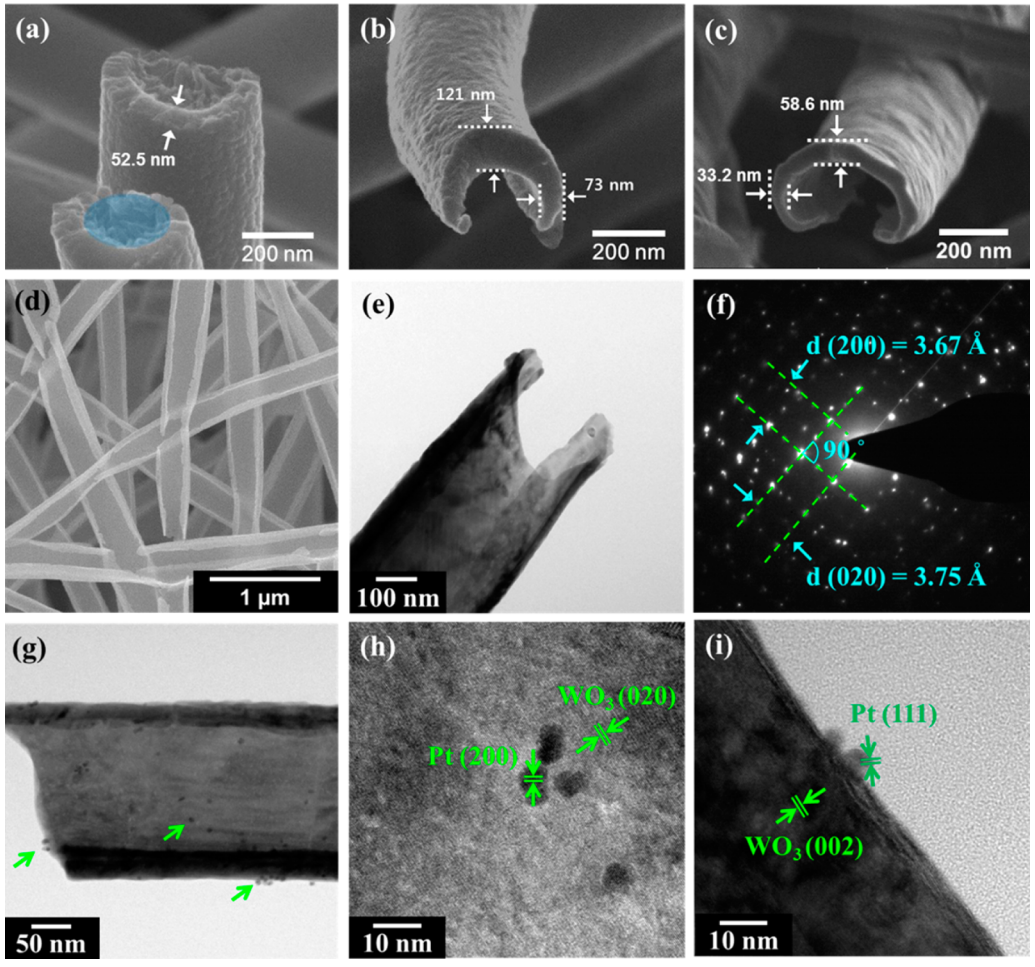

Figure 1. Morphologies and crystal structures of pristine WO_3 nanotubes and Pt-functionalized WO_3 hemitubes: (a) cross-sectional SEM image of the sputtered WO_3 films on fiber templates; (b, c) SEM image of WO_3 hemitubes with different top wall thicknesses of 121 and 58.6 nm, respectively; (d) SEM image of WO_3 hemitubes; (e) magnified TEM image of panel d; (f) selected area electron diffraction pattern of WO_3 hemitubes; (g) TEM image of Pt-functionalized WO_3 hemitube; and (h, i) magnified TEM image of panel g.

dx.doi.org/10.1021/ac303148a | *Anal. Chem.* 2013, 85, 1792−1796

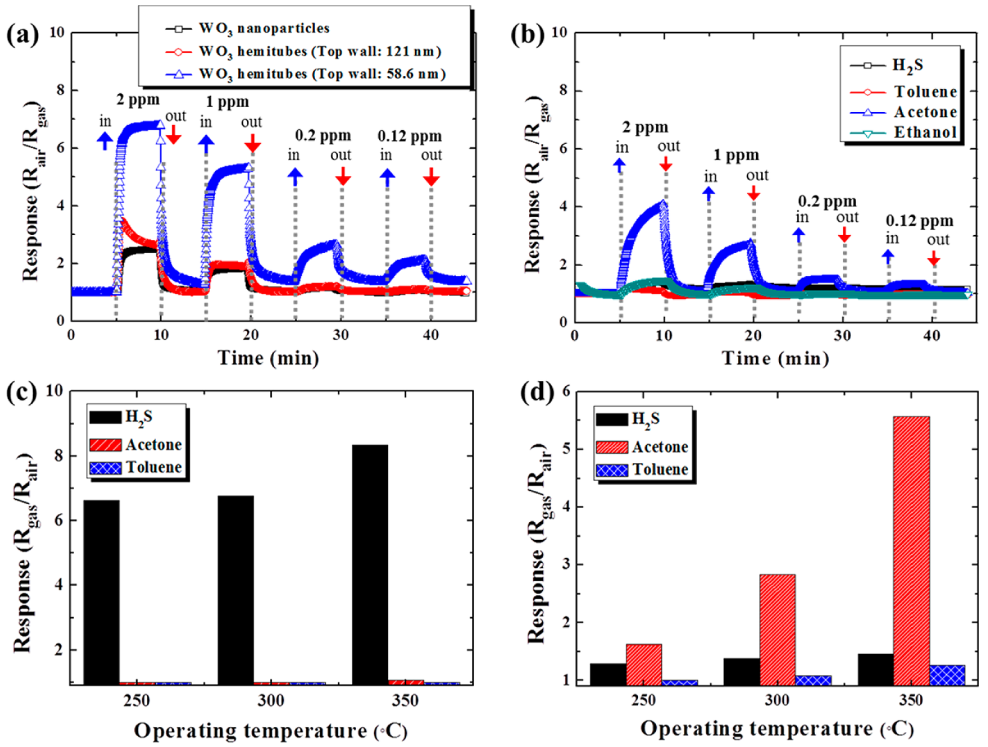

Figure 2. Gas sensor characterization: (a) response (R_{air}/R_{gas}) to H_2S gas at 300 °C; (b) response of Pt catalyst decorated WO_3 hemitubes at 300 °C; (c) response of pristine WO_3 hemitubes; and (d) Pt-functionalized WO_3 hemitubes in the temperature range of 250−350 °C.

individually. Pt particles had a cubic crystalline structure with (200) and (111) crystal planes, as indicated in Figure 1h and i.

X-ray diffraction (XRD) patterns of WO_3 hemitubes and WO_3 thin film were examined to identify the crystal orientations (Figure S4 in the Supporting Information). The WO_3 hemitubes exhibited a phase-pure monoclinic crystalline structure (JCPDS file no. 43-1035).

To investigate the exhaled-breath-sensing characteristics of pristine WO_3 and Pt-decorated WO_3 hemitubes, we carried out H_2S, acetone, toluene, and ethanol sensing tests using a homemade test setup (Figure S5 in the Supporting Information). WO_3 nanoparticles with a size distribution of 30−60 nm were drop-coated onto the sensing substrate and used as a reference sensing layer for comparison with WO_3 hemitubes with different wall thicknesses (Figure S3b in the Supporting Information and Figure 2a).

The average thicknesses of drop-coated sensing layers prepared using pristine WO_3 hemitubes, Pt-functionalized WO_3 hemitubes, and WO_3 nanoparticles were 72, 78.5, and 23.1 μm, respectively (see Figures S6 and S7 in the Supporting Information). The difference in the total thickness of the sensing layers consisting of WO_3 hemitubes and WO_3 nanoparticles originated from the high porosity of the hemitube structures. In their response to the H_2S gas, thinner WO_3 hemitubes having a 58.6 nm top wall thickness showed much enhanced sensing characteristics with stable resistivity changes (Supporting Information Figure S6). The gas response (R_{air}/R_{gas} at 2 ppm H_2S) of the 58.6 nm thick WO_3 hemitubes was 6.76, which indicates 1.94 and 2.72 times higher responses than those of 121 nm thick WO_3 hemitube- and WO_3 nanoparticle-based sensors, respectively.

The reaction mechanism of the WO_3 hemitubes to H_2S can be explained by the surface reaction between H_2S gas and adsorbed oxygen ions (O^-, O^{2-}), that is, $H_2S + 3O^- \rightarrow SO_2 + H_2O + 3e^-$.[23] The surface area of WO_3 hemitubes is approximately π (~3.14) times higher than that of planar dense thin films, leading to an enhanced surface reaction of the hemitube structure through its accommodation of a large number of O^- adsorption sites.[21] An increase in the density of the electron depletion region significantly improves the gas response. On the other hand, the gas response to acetone, toluene, and ethanol of the WO_3 hemitubes was negligible because of the complexity of the reaction (Figure S9 in the Supporting Information). In other words, reducing hydrogen species in acetone and ethanol are bound to carbon, which interrupts the dissociation of the molecules.[24,25] In addition, acetone and ethanol molecules need to experience several dissociation steps to be oxidized,[18,25] thus requiring more time to release ionized oxygen on the surface and inject electrons into the conduction band. In the case of toluene sensing, toluene molecules have a thermodynamically stable aromatic structure, which hinders the dissociation and oxidation of toluene at low temperatures (<450 °C).[26] These features led to outstanding selective detection toward H_2S.

Very interestingly, Pt-functionalized WO_3 hemitubes exhibited superior acetone-sensing characteristics with a response (R_{air}/R_{gas}) of 4.11 at 2 ppm, particularly showing a negligible response to H_2S, toluene, and ethanol (Figure 2b). The enhanced sensing properties to acetone of Pt-functionalized WO_3 hemitubes are ascribed to the spillover process[27] of Pt catalysts, which can effectively dissociate adsorbed oxygen molecules into ionized oxygens (O^-, O^{2-}) on the WO_3 surface, accompanied by the capture of electrons from the WO_3 conduction band. When acetone is exposed to Pt-functionalized WO_3 hemitubes, the adsorbed oxygen adions, which were effectively dissociated by the Pt catalysts, can be desorbed via surface reaction with acetone by the following eq 1 and 2 processes.[24]

dx.doi.org/10.1021/ac303148a | Anal. Chem. 2013, 85, 1792−1796

$$CH_3COCH_3(gas) + O^- \rightarrow CH_3COC^+H_2 + OH^- + e^- \quad (1)$$

$$CH_3COCH_3(gas) + 2O^- \rightarrow C^+H_3 + CO_2 + CH_3O^- + 2e^- \quad (2)$$

Accordingly, high resistivity changes toward acetone were detected (Figure S8 in the Supporting Information), whereas pristine WO_3 hemitubes did not show any noticeable response to acetone. The decrease in the H_2S response of the Pt-functionalized WO_3 hemitubes may be ascribed to the increased O^- density caused by the active spillover effect on the surface of Pt-functionalized WO_3 hemitubes at a high temperature (>200 °C), which hinders the resistivity changes[28] (Figure S10 in the Supporting Information). In addition, the low response to H_2S may stem from the catalytic filtering effect[29] of Pt nanoparticles, which decompose and oxidize H_2S before the gas reaches the active region, that is, the WO_3 surface. Thus, the resistivity changes of the Pt-functionalized WO_3 hemitubes were not noticeable against H_2S gas. This result demonstrates that the fabricated pristine WO_3 hemitubes and Pt catalyst functionalized WO_3 hemitubes showed superior cross sensitivity to H_2S and acetone. It was also confirmed that the superior cross sensitivity was observed in the wide temperature range of 250−350 °C, with increasing response at higher temperature (Figure 2c and d). The detection limit, which is the minimum detection gas concentration, was identified with the operating temperature at 300 °C. The detection limit was 120 ppb, showing a response of 1.23 for the WO_3 hemitubes to H_2S and 1.31 for Pt-functionalized WO_3 hemitubes to acetone, while exhibiting increased response in both sensing materials with concentration (Figure 3).

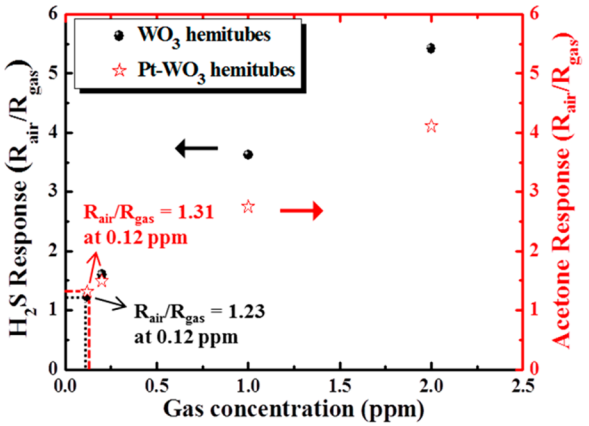

Figure 3. H_2S and acetone response (R_{air}/R_{gas}) to the pristine WO_3 hemitubes and Pt-functionalized WO_3 hemitubes, respectively, in the gas concentration ranges from 120 ppb to 2 ppm at 300 °C.

To investigate the long-term stability of gas sensors using pure WO_3 and Pt-functionalized WO_3 hemitubes, gas sensing tests with identical samples were performed after aging in air for 7 months. It is important to note that the superior selectivity of pristine WO_3 hemitubes and Pt-functionalized WO_3 hemitubes toward H_2S and acetone was maintained in the temperature range of 300 to 350 °C. Although the responses decreased for pristine WO_3 hemitubes to 3.44 ± 0.27 at 2 ppm of H_2S (a 49.1% decrease) while also decreasing for Pt-functionalized WO_3 hemitubes to 2.67 ± 0.53 for 2 ppm of acetone (6% decrease) at 300 °C, the response characteristics obtained after aging for 7 months were high enough for the selective detection of H_2S and acetone (Figure S11 and S12 in Supporting Information). This result demonstrates the high stability of our sensors.

In summary, thin-walled WO_3 hemitubes were synthesized by WO_3 sputtering deposition on polymer nanofiber templates, followed by high-temperature calcination. The wall thickness was easily manipulated by changing the sputtering time, leading to more effective surface modulation in the case of thinner-walled WO_3 hemitubes. From the gas-sensing characterization, pristine WO_3 hemitubes showed superior H_2S sensing properties with minimal response to acetone and toluene at 85 RH%. Catalytic Pt nanoparticles were decorated on WO_3 hemitubes to modulate gas response characteristics. Pt-functionalized WO_3 hemitubes showed superior acetone response (R_{air}/R_{gas} = 4.11 at 2 ppm) with negligible H_2S response, and pristine WO_3 hemitubes exhibited a 4.90-fold sensitivity toward H_2S with minimal acetone-sensing characteristics. From the cyclic test of pristine WO_3 hemitubes and Pt-functionalized WO_3 hemitubes after 7 months, the outstanding selectivity characteristics were confined to H_2S and acetone, respectively. The highly sensitive and selective acetone-sensing properties of Pt-functionalized WO_3 hemitubes offer a potential platform for application in diabetes diagnosis by measuring traces of acetone gas in human breath.

■ ASSOCIATED CONTENT

Supporting Information

Preparation of hollow WO_3 hemitubes, transmission electron microscopy (TEM) analysis, X-ray diffraction (XRD) analysis, preparation of sensing material, gas sensor test setup, gas sensing characteristics, and long-term stability of the sensing performance. This material is available free of charge via the Internet at http://pubs.acs.org.

■ AUTHOR INFORMATION

Corresponding Author

*E-mail: idkim@kaist.ac.kr.

Notes

The authors declare no competing financial interest.

■ ACKNOWLEDGMENTS

I.D.K. acknowledges the support by the Engineering Research Center (ERC-N01120073) Program from the Korean National Research Foundation. This work was also supported by the Center for Integrated Smart Sensors funded by the Ministry of Education, Science and Technology as Global Frontier Project (CISS-2012M3A6A6054188).

■ REFERENCES

(1) Phillips, M.; Gleeson, K.; Hughes, J. M. B.; Greenberg, J.; Cataneo, R. N.; Baker, L.; McVay, W. P. *Lancet* **1999**, *353*, 1930−1933.

(2) O'Neill, H. J.; Gordon, S. M.; O'Neill, M. H.; Gibbons, R. D.; Szidon, J. P. *Clin. Chem.* **1988**, *34*, 1613−1618.

(3) Yu, H.; Xu, L.; Cao, M.; Chen, X.; Wang, P.; Jiao, J.; Wang, Y. *Proc. IEEE Sens.* **2003**, *2*, 1333−1337.

(4) Kamat, P. C.; Roller, C. B.; Namjou, K.; Jeffers, J. D.; Faramarzalian, A.; Salas, R.; McCann, P. J. *Appl. Opt.* **2007**, *46*, 3969−3975.

(5) Turner, C.; Walton, C.; Hoashi, S.; Evans, M. *J. Breath Res.* **2009**, *3*, 046004.

(6) Wertz, Z. W.; Birnbaum, A. J.; Sobotka, P. A.; Zaring, E. J.; Skosey, J. L. *Lancet* **1991**, *337*, 933−935.
(7) Lemoyne, M.; Gossum, A. V.; Kurian, R.; Jeejeebhoy, K. N. *Am. J. Clin. Nutr.* **1988**, *48*, 1310−1315.
(8) Narasimhan, L. R.; Goodman, W.; Kumar, C.; Patel, N. *Proc. Natl. Acad. Sci. U.S.A.* **2001**, *98*, 4617−4621.
(9) Kharitonov, S.; Alving, K.; Barnes, P. J. *Eur. Respir. J.* **1997**, *10*, 1683−1693.
(10) Righettoni, M.; Tricoli, A.; Pratsinis, S. E. *Anal. Chem.* **2010**, *82*, 3581−3587.
(11) Wang, L.; Teleki, A.; Pratsinis, S. E.; Gouma, P. I. *Chem. Mater.* **2008**, *20*, 4794−1496.
(12) Gouma, P.; Prasad, A.; Stanacevic, S. *J. Breath Res.* **2011**, *5*, 037110−037110.
(13) Ryabtsev, S. V.; Shaposhnick, A. V.; Lukin, A. N.; Domashevskaya, E. P. *Sens. Actuators B* **1999**, *59*, 26−29.
(14) Chang, Y. E.; Youn, D. Y.; Ankonina, G.; Yang, D. J.; Kim, H. G.; Rothschild, A.; Kim, I. D. *Chem. Commun.* **2009**, *27*, 4019−4021.
(15) Cho, N. G.; Woo, H. S.; Lee, J. H.; Kim, I. D. *Chem. Commun.* **2011**, *47*, 11300−11302.
(16) Gouma, P.; Kalyanasundaram, K.; Yun, X.; Stanacevic, M.; Wang, L. *IEEE Sens. J.* **2010**, *10*, 49−53.
(17) Moon, J.; Park, J. A.; Lee, S. J.; Zyung, T.; Kim, I. K. *Sens. Actuators B* **2010**, *149*, 301−305.
(18) Shin, J.; Choi, S. J.; Youn, D. Y.; Kim, I. D. *J. Electroceram.* **2012**, *29*, 106−116.
(19) Seo, M. H.; Yuasa, M.; Kida, T.; Kanmura, Y.; Huh, J. S.; Yamazoe, N.; Shimanoe, K. *J. Ceram. Soc. Jpn.* **2011**, *119*, 884−889.
(20) Yang, D. J.; Kamienchick, I.; Youn, D. Y.; Rothschild, A.; Kim, I. D. *Adv. Funct. Mater.* **2010**, *20*, 4258−4264.
(21) Choi, S. H.; Ankonina, G.; Youn, D. Y.; Oh, S. G.; Hong, J. M.; Rothschild, A.; Kim, I. D. *ACS Nano* **2009**, *3*, 2623−2631.
(22) Bonet, F.; Delmas, V.; Grugeon, S.; Urbina, R. H.; Silvert, P. Y.; Tekaia-Elhsissen, K. *Nanostruct. Mater.* **1999**, *11*, 1277−1284.
(23) Rout, C. S.; Hegde, M.; Rao, C. N. R. *Sens. Actuators B* **2008**, *128*, 488−493.
(24) Khadayate, R. S.; Sali, J. V.; Patil, P. P. *Talanta* **2007**, *72*, 1077−1081.
(25) Wang, Y.-D.; Chen, Z.-X.; Li, Y.-F.; Zhou, Z.-L.; Wu, X.-H. *Solid-State Electron.* **2001**, *45*, 639−644.
(26) Nakamura, Y.; Morita, Y.; Ishikura, Y.; Takagi, H.; Fujitsu, S. *Advances in Chemical Sensors: Photo-Assisted Organic Pollutants Sensing by a Wide Gap pn Heterojunction*; InTech; Croatia, 2011, p 236.
(27) Matsushima, S.; Teraoka, Y.; Miura, N.; Yamazoe, N. *Jpn. J. Appl. Phys.* **1988**, *27*, 1798−1802.
(28) Tao, W.-H.; Tsai, C.-H. *Sens. Actuators B* **2002**, *81*, 237−247.
(29) Portnoff, M. A.; Grace, R.; Guzman, A. M.; Runco, P. D.; Yannopoulos, L. N. *Sens. Actuators B* **1991**, *5*, 231−235.